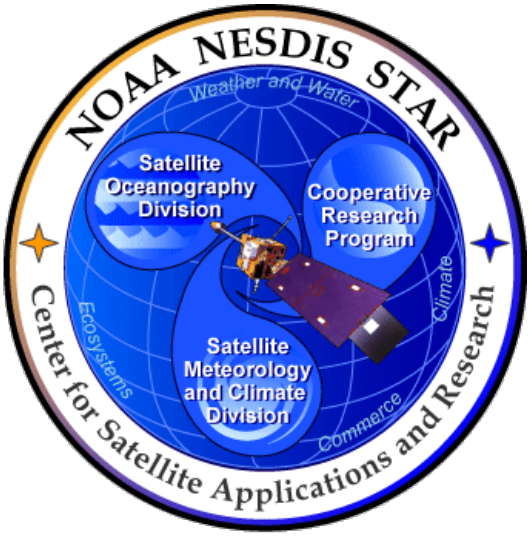

NOAA NESDIS

CENTER for SATELLITE APPLICATIONS and RESEARCH

ALGORITHM THEORETICAL BASIS DOCUMENT

Ice Surface Temperature, Ice Concentration, and Ice Cover from VIIRS, ABI, and METimage

Yinghui Liu, UW/CIMSS

Jeffrey R. Key, NOAA/NESDIS/STAR

Version 1.4

15 June 2020

TABLE OF CONTENTS

LIST OF FIGURES

LIST OF TABLES

LIST OF ACRONYMS

ABI: Advanced Baseline Imager
AIT: Algorithm Integration Team
AITA: AIT Algorithm
AMSR2: Advanced Microwave Scanning Radiometer 2
AMSR-E: Advanced Microwave Scanning Radiometer - Earth Observing System
ATBD: Algorithm Theoretical Basis Document
AVHRR: Advanced Very High Resolution Radiometer
AWG: Algorithm Working Group
CIMSS: Cooperative Institute for Meteorological Satellite Studies
DMSP: Defense Meteorological Satellite
EASE-Grid: Equal-Area Earth Grid
EPS-SG: EUMETSAT Polar System-Second Generation
FOV: Field of View
GOES-R: Geostationary Operational Environmental Satellite R series
IST: Ice Surface Temperature
JPSS: Joint Polar Satellite System
MODIS: Moderate Resolution Imaging Spectroradiometer
MRD: Mission Requirements Document
MS2GT: MODIS Swath-to-Grid Toolbox
MSG: Meteosat Second Generation
NASA: National Aeronautics and Space Administration
NDSI: Normalized Difference Snow Index
NOAA: National Oceanic and Atmospheric Administration
OLI: Operational Land Imager
RMSE: Root Mean Squared Error
SEVIRI: Spinning Enhanced Visible and Infrared Imager
S-NPP: Suomi National Polar Orbiting Partnership
SSMIS: Special Sensor Microwave Imager/Sounder
TIRS: Thermal Infrared Sensor
TOA: Top of atmosphere
USGS: U.S. Geological Survey
VII: Visible Infrared Imager
VIIRS: Visible Infrared Imaging Radiometer Suite

ABSTRACT

Sea and lake ice influence the surface radiation budget and affects energy and moisture exchange between the atmosphere and the underlying water. It is one of the key factors to consider in the atmospheric circulation, numerical weather forecasting, and climate models. Information of ice cover is also important for planning commercial transport. Ice cover and concentration are among the most important indices in studying climate change. Accurate retrievals of ice cover and concentration are of high importance both to the scientific communities and to the general public. This document provides a detailed description of the physical basis and technical approach of the algorithm to identify ice cover and estimate ice concentration and ice surface temperature over water surfaces under clear-sky conditions. Linear regression is used to retrieve ice surface temperature from satellite observations with split window channels. A group threshold method is applied to identify ice over water surfaces and a tie-point algorithm is carried out to determine the representative reflectance/temperature of 100% ice covered surface, which is then used to estimate the ice concentration. This algorithm can be applied to multiple sensors on multiple satellite platforms, e.g. the Advanced Baseline Imager (ABI) on the Geostationary Operational Environmental Satellite R series (GOES-R) of National Oceanic and Atmospheric Administration (NOAA) geostationary meteorological satellites, the Visible Infrared Imaging Radiometer Suite (VIIRS) onboard the Suomi National Polar Orbiting Partnership (S-NPP), and the Joint Polar Satellite System (JPSS), and the METimage (also called Visible Infrared Imager or VII) to be integrated in the EUMETSAT Polar System-Second Generation (EPS-SG) or Metop SG. Validations of retrieval products using proxy data of GOES-R ABI, and observations from GOES-R ABI and S-NPP VIIRS show that the results meet the requirements of product measurement accuracy and precision.

1 Introduction

1.1 Purpose of This Document

The ice cover and concentration algorithm theoretical basis document (ATBD) provides a detailed description of the physical basis and technical approach for the identification of ice cover and estimation of ice concentration and ice surface temperature (IST). These retrievals are over water surfaces, including ocean water and fresh water, under clear-sky conditions. This algorithm can be applied to but not limited to the Advanced Baseline Imager (ABI) on the Geostationary Operational Environmental Satellite R series (GOES-R) of National Oceanic and Atmospheric Administration (NOAA) geostationary meteorological satellites, the Visible Infrared Imaging Radiometer Suite (VIIRS) onboard the Suomi National Polar Orbiting Partnership (S-NPP), and the Joint Polar Satellite System (JPSS)), and the METimage (also called Visible Infrared Imager or VII) to be integrated in the EUMETSAT Polar System-Second Generation (EPS-SG) or Metop SG. The water surfaces include inland lakes, rivers and oceans. No land ice applications are included. Output of this algorithm is available to other algorithms, which require knowledge of the ice information. The ice information is also important for planning commercial transportation, short-term weather forecasting, water management, and damage control. Long-term records of ice cover and concentration data are valuable for climate change studies.

1.2 Who Should Use This Document

Intended users of this document are those interested in understanding the physical basis and technical approach of the algorithm and applying the products of this algorithm for their particular purpose. This document also provides information useful to anyone to implement, maintain and improve the original algorithm.

1.3 Inside Each Section

This document is broken down into the following main sections.

- **System Overview**: Provides relevant details of the satellite instruments, and a brief description of the products to be generated by this algorithm.
- **Algorithm Description**: Provides the detailed description of the algorithm including its physical basis, technical approach, required input, and output.
- **Assumptions and Limitations**: Provides an overview of the assumptions, limitations of current approach.

1.4 Related Documents

None.

1.5 Revision History

Version 1.4 of this document was created by Yinghui Liu and Jeff Key, NOAA/NESDIS/STAR. This version adds JPSS VIIRS and Metop-SG METimage.

2 Observing System Overview

This algorithm can be applied to multiple sensors on multiple satellite platforms. Among those platforms, there are ABI on GOES-R, VIIRS on S-NPP and JPSS, and METimage on EPS-SG. This section will describe instrument characteristics of ABI, VIIRS, and METimage, and products of this algorithm.

2.1 Instrument Characteristics

The ABI onboard the future GOES-R has a wide range of applications in weather, oceanographic, climate, and environmental studies. ABI has 16 spectral bands (Table 1), with 2 visible bands, 5 near-infrared bands, and 9 infrared bands. The spatial resolution of ABI will be nominally 2 km for the infrared bands, 1 km for 0.47, 0.86, and 1.61 μm bands, and 0.5 km for the 0.64 μm visible band. ABI will scan the full disk every 15 minutes, plus continental United States 3 times, plus a selectable 1000 km × 1000 km area every 30 s. ABI can also be programmed to scan the full disk every 5 minutes. Compared to previous GOES imagers, ABI offers more spectral bands and better spatial resolution. Especially, the newly added bands at 1.61 μm, and higher spatial resolution at 0.64 μm allows for a better detection and monitoring of surface snow and ice (Schmit et al. 2005).

Table 1. *ABI band numbers and wavelengths.*

Band Number	***Wavelength (μm)***	***Subsatellite Field of View (km)***	***Used in Ice Algorithms***
1	0.47	1	
2	0.64	0.5	Yes
3	0.86	1	Yes
4	1.38	2	
5	1.61	1	Yes
6	2.26	2	
7	3.9	2	
8	6.15	2	
9	7.0	2	
10	7.4	2	
11	8.5	2	
12	9.7	2	
13	10.35	2	
14	11.2	2	Yes
15	12.3	2	Yes
16	13.3	2	

The VIIRS onboard the S-NPP and the JPSS satellites has 22 spectral bands covering wavelengths from 0.4 to 11.8 μm (Table 2). The S-NPP was launched on October 28, 2011; the first JPSS satellite, JPSS-1, was launched on November 18, 2017. Among the 22 bands, there are 5 high resolution imagery bands (I-bands, 375 m spatial resolution at nadir), 16 moderate resolution bands (M-bands, 750 m spatial resolution at nadir), and one Day/Night Band (DNB, 750 m spatial resolution). The VIIRS swath width is 3000 km.

Table 2. *VIIRS band numbers and wavelengths.*

Band Number	***Wavelength (μm)***	***Subsatellite Field of View (km)***	***Used in Ice Algorithms***
M1	0.411	0.750	
M2	0.444	0.750	
M3	0.486	0.750	
M4	0.551	0.750	
I1	0.639	0.375	
M5	0.672	0.750	Yes
M6	0.745	0.750	
I2	0.862	0.375	
M7	0.862	0.750	Yes
M8	1.238	0.750	
M9	1.375	0.750	
I3	1.602	0.375	
M10	1.602	0.750	Yes
M11	2.257	0.750	
I4	3.753	0.375	
M12	3.697	0.750	
M13	4.067	0.750	
M14	8.578	0.750	
M15	10.729	0.750	Yes
I5	11.469	0.375	
M16	11.845	0.750	Yes
DNB	0.7	0.750	

METimage is an advanced multispectral imaging radiometer for meteorological applications. It is a follow-on to Advanced Very High Resolution Radiometer (AVHRR) on MetOp in the mid morning orbit. METimage will be integrated in the EPS-SG to be operational by 2022. The

METimage has 20 spectral channels from 0.4 to 13.4 μm (Table 3), with several water vapor channels that VIIRS does not. METiamge swath width is about 2800 km, with a ground sampling distance of 500 m. Simulated METimage data, provided by EUMETSAT, are based on AVHRR product for clouds, Monitoring Atmospheric Composition and Climate (MACC) reanalysis for aerosols, ECMWF reanalysis for atmospheric state, and MOIDS albedo climatology, and simulated by the radiative transfer model of ARTDECO (Laboratoire d'Optique Atmosphérique at the Université de Lille-1).

Table 3. *METimage (VII) channel numbers and wavelengths.*

Channel Number	***Wavelength (μm)***	***Bandwidth (μm)***	***Used in Ice Algorithms***
VII-4	0.443	0.03	
VII-8	0.555	0.02	
VII-12	0.670	0.02	Yes
VII-15	0.752	0.01	
VII-16	0.763	0.01	
VII-17	0.865	0.02	Yes
VII-20	0.914	0.02	
VII-22	1.240	0.02	
VII-23	1.375	0.04	
VII-24	1.630	0.02	Yes
VII-25	2.250	0.05	
VII-26	3.740	0.18	
VII-28	3.959	0.06	
VII-30	4.050	0.06	
VII-33	6.735	0.37	
VII-34	7.325	0.29	
VII-35	8.540	0.29	
VII-37	10.690	0.50	Yes
VII-39	12.020	0.50	Yes
VII-40	13.345	0.31	

Inputs of this algorithm include observations at 0.64 μm, 0.86 μm, 1.6 μm, and split window channels, which are band 2, 3, 5, 14, and 15 for ABI, M5, M7, M10, M15, and M16 for VIIRS, and VII-12,VII-17, VII-24, VII-37, and VII-39 for METimage.

2.2 Products Generated

The ice cover, ice concentration, and IST algorithm is responsible for identification of pixels covered with ice over water surfaces under clear-sky conditions, and for estimation of ice concentration and IST. No land ice applications are included.

Table 4. *GOESR-R ABI product function and performance specifications for ice cover, concentration, and surface temperature.*

GOES-R ABI Sea/Lake Ice Concentration/Extent/IST product capabilities	
Satellite Source	GOES-16 ABI
Accuracy/Precision	Cover: 85% probability of correct ice detection Concentration: 10% accuracy; 25% precision IST: 1 K
Measurement Range	0 - 100%, for Ice Concentration Ice, non-ice and invalid pixel mask, for Ice Extent 213 - 275 K, Ice Surface Temperature
Latency	3236 sec
Timeliness	3236 sec
Refresh	3 hours
Coverage	FD
Horizontal Resolution	FD – 2 km
Cloud Cover Conditions Qualifier	Clear Conditions associated with threshold accuracy
Temporal Qualifier	Ice Covered waters; Day and Night Day with sun at less than 67 degree solar zenith angle
Product Extent Qualifier	Quantitative out to at least 67 degrees LZA and qualitative at larger LZA (Note: AICE is processed out to LZA = 80 degrees)

Ice cover is the location of ice over inland lakes, rivers, and ocean waters; and ice concentration reports the fraction (in percentages) of the ice for those ice-covered pixels; and IST reports the temperature of those ice-covered pixels. The ice cover mask is generated for each pixel over water surface, and ice concentration and IST are calculated for each pixel covered with ice. All products are for pixels under clear-sky condition only. This algorithm relies on the accuracy of other dependent products including cloud mask, land/water mask, and etc. Details of the required input parameters and product validations are presented in the following sections. The required product Function and Performance Specification (F&PS) for ice cover and ice concentration of GOESE-R ABI are listed in Table 4, and for ice concentration and IST from VIIRS in Tables 5 and 6.

Table 5. *JPSS product function and performance specification for ice concentration for VIIRS.*

JPSS RRPS Sea Ice Concentration Supplement Requirements Table		
User & Priority	**JPSS3**	
Attribute	**Threshold**	**Objective**
Geographic Coverage	All ice-covered regions of the global ocean	
Vertical Coverage	Ice Surface	Ice Surface
Horizontal Cell Size	Clear: 1.0 km All weather: no capability	Clear: 0.5 km All weather: 1 km
Measurement Range	0 – 100%	
Mapping Uncertainty, 3 Sigma	Clear: 1 km at nadir Cloudy: No capability	Clear: 0.5 km Cloudy: 1 km
Measurement Accuracy	10%	
Measurement Uncertainty	25%	
Product Refresh Rate	At least 90% coverage of the globe every 24 hours (monthly average)	6 hrs
Latency	30 minutes after granule data is available	
Timeliness	≤ 3hours	

Table 6. *JPSS product function and performance specification for ice surface temperature for VIIRS.*

JPSS RRPS Ice Surface Temperature Supplement Requirements Table		
User & Priority	**JPSS4**	
Attribute	**Threshold**	**Objective**
Geographic Coverage	All ice-covered regions of the global ocean	
Sensing Depth	Ice Surface	Ice Surface
Horizontal Cell Size	Nadir - 1km Worst Case –1.6 km	Nadir - 0.1km Worst Case – 0.1 km
Measurement Range	213 - 275 K	213 - 293 K (2 m above ice)
Mapping Uncertainty, 3 Sigma	Clear: 1 km at nadir Cloudy: No capability	Clear: 0.5 km Cloudy: 1 km
Measurement Uncertainty	1 K	1 K
Product Refresh Rate	At least 90% coverage of the globe every 24 hours (monthly average)	6 hrs
Latency	30 minutes after granule data is available	
Timeliness	≤ 3hours	

3 Algorithm Description

3.1 Algorithm Overview

This automated algorithm detects ice cover and retrieves ice concentration and IST. Ice cover is first determined by a group threshold method. Then ice concentration is retrieved based on the determined normalized reflectance/temperature of pure ice and pure water through application of a tie point algorithm. IST is retrieved using a linear regression approach.

Pros: This automated algorithm is designed on solid physical foundation and is capable of identifying ice cover and retrieving concentration for both day and nighttime under clear-sky conditions. It runs automatically and can be employed globally.

Cons: The accuracy of this algorithm depends on the quality of the cloud mask, and no retrieval can be carried out for cloudy pixels.

3.2 Processing Outline

The processing outline of this algorithm is summarized in Figure 1.

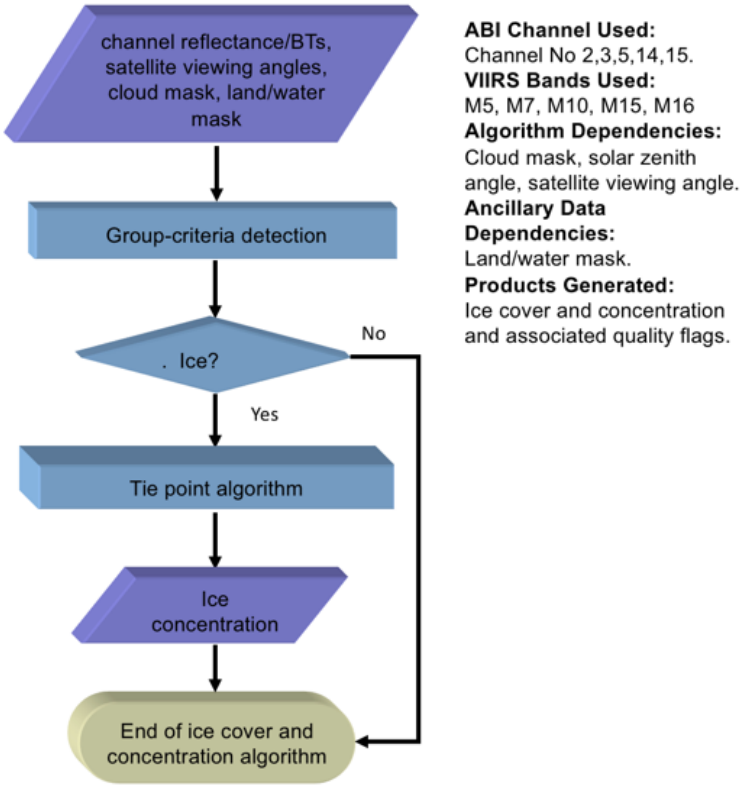

Figure 1. *High level flowchart of the ice cover and concentration algorithm illustrate the main processing sections.*

3.3 Algorithm Input

This section describes the input of this ice cover and concentration algorithm.

3.3.1 Input Data

The list below contains the primary input data used in this algorithm, include sensor data, satellite derived products, and ancillary data. The primary sensor data are:

- Reflectances of VIIRS M-bands 5, 7, and 10, GOES-R ABI band 2, 3, and 5, which are at 0.64 μm, 0.86 μm, and 1.6 μm
- Brightness Temperatures in VIIRS M-band 15 and 16, GOES-R ABI band 14 and 15, which are 11 μm, and 12 μm
- Latitude and Longitude
- Sensor viewing zenith angle
- Local zenith angle
- Solar zenith angle

The satellite derived products include:

- Cloud mask

Ancillary data are data that requires information not included in the satellite observations or derived products. The ancillary data include:

- Land mask

The pixel level spatial resolution of ABI band 2, 3, 5, 14, and 15 are 0.5 km, 1 km, 1 km, 2 km, and 2 km at sub-satellite field of view (FOV), and 0.750 km sub-satellite FOV for VIIRS M5, M7, M10, M15, and M16 bands. The required horizontal resolution of the ABI outputs is at 2 km for ice cover and ice concentration retrievals, and 1km for VIIRS sea ice cover, ice concentration, and IST. This algorithm of this version is capable of producing outputs with the spatial resolution at 2 km for ABI, and at 0.750 km for VIIRS.

Both the VIIRS and ABI cloud mask are 4-level cloud mask, clear, probably clear, probably cloudy, and cloudy. Cloud mask input of this algorithm includes two categories: clear (clear and probably clear in cloud mask of VIIRS and ABI cloud mask), and cloudy (cloudy and probably cloudy of VIIRS and ABI cloud mask). No retrievals are performed for pixels of cloud shadow or sun glint. The cloud shadow and sun glint information are available from VIIRS cloud mask. When cloud shadow and sun glint information are not available, e.g. from GOES-R, pixels are assumed under conditions of no cloud shadow or sun glint.

Land mask comes from the geolocation data. There are total four values in the current land mask as input, i.e. 0, 1, 2, and 3. Value 0 represents the ocean water surface, including shallow ocean (ocean is less than 5 kilometers from the coast or with depth less than 50 meters), moderate or continental ocean (ocean is more than 5 kilometers from the coast and with depth between 50 and 500 meters), and deep ocean (depth larger than 500 meters); value 1 stands for in-land water surface, including shallow inland water (inland water less than 5 kilometer from shoreline or depth less than 50 meters), ephemeral water, and deep inland water (inland water more than 5 kilometer from shoreline and depth more than 50 meters); value 2 means land surface, including

land, ocean coastlines, and lake shorelines; value 3 includes all other pixels, including bow-tie delete pixels.

3.4 Theoretical Description of Algorithm

In the following sections, the physical background and technical approaches of the processes in this algorithm are described.

3.4.1 Physics of the Problem

3.4.1.1 Ice and snow reflectance

Ice surface reflectance depends strongly on its internal structure, such as brine pockets, air bubbles of the near surface layers. These internal structures change with season, state of the near surface layers, and age of ice, which results in different ice types. Reflectance of ice surface is different from that of snow surface. Ice consists mainly of sheets, while snow consists of grains. Absorption and scattering in the snow and ice surface are determined by their internal inhomogeneities (Grenfell and Maykut, 1977). Reflectance of snow, snow-covered ice, and ice surfaces shows very high values at visible channels, but low values at short-wavelength channels longer than 1.4 microns (Bolsenga 1983), due to the much stronger absorption and much less back scattering at those infrared channels; most of the ice and snow-covered ice surfaces show higher reflectance at visible and near infrared channels than water surface. These features can be used to detect ice cover over water surfaces. Other substances do not have this unique spectral signature of snow and ice. Clouds have high reflectance at both visible and near infrared channels. Water surface is dark at all wavelengths (Riggs et al. 1999). However, some ice types, such as clear lake ice, grease ice, can be difficult to detect for their very low contrast with open water.

3.4.1.2 Ice surface temperature

IST under clear-sky conditions is retrieved using brightness temperatures at split window channels, which are ABI band 14 and 15, and VIIRS band M15 and M16. One window channel, so called clean window channel, is in the electromagnetic spectrum where there is very little water vapor absorption (ABI band 14, VIIRS band M15); another window channel, so called dirty window channel, has modest amounts of water vapor absorption (ABI band 15, VIIRS band M16). The retrieval algorithm is from the work of Key et al. (1997). IST is retrieved using the following equation.

$$Ts = a + bT11 + cT12 + d\,[(T11-T12)(\sec\theta-1)] \qquad (1)$$

where Ts is the estimated IST (Unit: Kelvin), and T11 and T12 are the brightness temperatures (K) of the two split window channels. θ is the sensor scan angle for sensors onboard the polar-orbiting satellites, e.g. AVHRR, MODIS, and VIIRS; because of the very small range of sensor scan angle of the geostationary satellite sensors, e.g. ABI, the local zenith angle θ is used instead of the sensor scan angle. Coefficients a, b, c, and d are derived for the following temperature ranges: T11 < 240K, 240K < T11 < 260K, T11 > 260K. The coefficients are based on modeled radiances in the split window channels using Arctic and Antarctic temperature and humidity profiles, and angular emissivity models for snow. See Key et al. (1997) for additional details. It

should be not that this method is specifically designed for the skin temperature retrievals over ice/snow surface, which is not provided from the land team.

The coefficients for the current S-NPP VIIRS, JPSS-1 VIIRS, GOES-R ABI, and EPS-SG METimage proxy data are included in Table 7, 8, 9, 10. The coefficients for ESP-SG METiamge are currently the same as those of S-NPP VIIRS, and they will be updated once the METimage spectral response functions become available. In equation (1), the sensor scan angle is derived from the sensor zenith angel using the following equation.

$$\theta = \arcsin(\sin(\lambda) \times R_e / (R_e + A_{sat})) \qquad (2)$$

where λ is the sensor zenith angle, R_e is the equatorial radius of the Earth, A_{sat} is the nominal altitude of the satellite.

Table 7. *Values of coefficients a, b, c, and d in equation (1) for S-NPP VIIRS*

Temperature Range		a	b	c	d
Northern Hemisphere	< 240 K	-7.335613	1.030383	1.264255	-0.438851
	240 – 260 K	-8.606919	1.03532	0.641668	1.838797
	> 260 K	-6.629177	1.027197	1.082237	2.159417
Southern Hemisphere	< 240 K	-2.288466	1.010255	-0.123422	0.389902
	240 – 260 K	-9.375047	1.03893	-0.3151	2.575988
	> 260 K	-8.715563	1.035604	0.425955	2.378302

Table 8. *Values of coefficients a, b, c, and d in equation (1) for JPSS-1 VIIRS*

Temperature Range		a	b	c	d
Northern Hemisphere	< 240 K	-7.158368	1.029460	1.422872	-0.586471
	240 – 260 K	-8.332039	1.034038	0.803878	1.497199
	> 260 K	-6.404185	1.026105	1.123782	1.908568
Southern Hemisphere	< 240 K	-2.279740	1.010068	0.058146	0.246515
	240 – 260 K	-9.248563	1.038296	-0.126050	2.199003
	> 260 K	-8.641733	1.035160	0.498707	2.111319

Table 9. *Values of coefficients a, b, c, and d in equation (1) for GOES-R ABI*

Temperature Range		a	b	c	d
Northern Hemisphere	< 240 K	3.439249	0.985022	0.725899	0.037636
	240 – 260 K	1.344560	0.993557	0.774645	0.020610

	> 260 K	-4.932469	1.015409	1.095950	0.019513
Southern Hemisphere	< 240 K	1.177880	0.994992	0.502566	0.070178
	240 – 260 K	1.408750	0.993496	0.705781	0.025485
	> 260 K	-4.158840	1.013769	0.896800	0.028608

Table 10. *Values of coefficients a, b, c, and d in equation (1) for EPS-SG METimage proxy data*

Temperature Range		a	b	c	d
Northern Hemisphere	< 240 K	-7.335613	1.030383	1.264255	-0.438851
	240 – 260 K	-8.606919	1.03532	0.641668	1.838797
	> 260 K	-6.629177	1.027197	1.082237	2.159417
Southern Hemisphere	< 240 K	-2.288466	1.010255	-0.123422	0.389902
	240 – 260 K	-9.375047	1.03893	-0.3151	2.575988
	> 260 K	-8.715563	1.035604	0.425955	2.378302

3.4.2 Mathematical Description

3.4.2.1 Ice detection

Ice cover is detected at the pixel level over water surface under clear-sky conditions. Snow covered ice show high reflectance in the visible channels, and very low reflectance in shortwave infrared channels, and many ice types also have this characteristic. Most ice types have higher reflectance than open water, which typically has a very low reflectance.

Traditionally, the Normalized Difference Snow Index (NDSI) is used to detect snow and ice. NDSI is defined as

$$NDSI = (R_1 - R_2)/(R_1 + R_2) \qquad (3)$$

where R_1 is often the reflectance in visible channel, (e.g. 0.55 μm for MODIS), R_2 is the reflectance in shortwave infrared channel (e.g. 1.6 or 2.1 μm for MODIS). Ice is identified when NDSI is larger than a preset threshold. In this algorithm, 0.86 μm and 1.6 μm bands are selected for R_1 and R_2, band M7 and M10 for VIIRS, and band 3 and 5 for ABI. Both bands have the same spatial resolution for ABI (1km at sub-satellite FOV) and VIIRS (0.750 km at sub-satellite FOV). Furthermore, one advantage of 0.865 μm over 0.55 μm to calculate NDSI is that NDSI calculated using 0.55 μm reflectance is higher than preset threshold over water surfaces in some cases, while NDSI from 0.865 μm is mostly lower than the preset threshold. Another characteristic of ice is that ice cover has colder surface temperature than water melting point. Water with higher salinity usually has lower melting temperature.

During the daytime (solar zenith angle lower than 85 degree), a pixel is identified as possible ice covered if 1) the NDSI value is larger than a threshold, 0.45 for VIIRS and 0.6 for ABI, 2) the reflectance at 0.865μm, VIIRS band M7 and ABI band 3, higher than 0.08 (Hall et al. 2001, 2006), and 3) surface temperature lower than preset thresholds (275 K over both fresh water salty and ocean water). The reason not to use the melting temperature, 273.15 K for fresh water and 271.5 K for salty ocean water with salinity of 35 PSU, is that some ice-covered pixels with melting water have surface temperature higher than water melting point.

During the nighttime (solar zenith angle higher than or equal to 85 degree), a pixel is identified as possible ice covered if surface temperature is lower than 275.0 K over lake or river (fresh water), and over ocean (salty) water.

3.4.2.2 Ice concentration from tie points algorithm

Ice characteristics change temporally and spatially. Different ice types can appear simultaneously in a large field of view and change over time. Under certain conditions that a single ice type appears in a specific area, surface reflectance or temperature of the pure ice, 100% ice covered, is the same, while distinct from open water. Spatial variations in surface reflectance/temperature in this area are mainly due to changing ice concentrations, fraction of the surface covered by ice. In regard to satellite view, a single ice type can exist in a search window of a certain shape (a square or a circle) and size, e.g. length of the square in pixels. Theoretically, the reflectance and temperature of pure ice and open water can be derived from a tie point method in a search window, if 100% ice covered pixels are the majority of all ice-covered pixels, including 100% ice covered pixels and partially ice-covered pixels, in the search window (Figure 2a, 2b).

Then, ice concentration for a pixel (F_p) inside the search window can be calculated by

$$F_p = (B_p - B_{water}) / (B_{ice} - B_{water}) \qquad (4)$$

where B_{water} is the reflectance/temperature of pure water pixels, B_{ice} is the reflectance/temperature of pure ice pixels; B_p is the observed reflectance/temperature of the pixel, of which ice concentration will be calculated. In the current version of this algorithm, reflectance at 0.64 μm at the top of atmosphere, VIIRS band M5 and ABI band 2, is selected in daytime, and surface skin temperature is selected at nighttime. Surface skin temperature can also be used in daytime, and whether the final ice concentration in daytime uses only the retrievals from reflectance, or only the retrievals from surface skin temperature, or the optimal combination of both retrievals need further investigation. For VIIRS, the spatial resolution is 0.750 km; for ABI, the spatial resolution is 0.5 km at 0.64 μm band, and 2.0 km for surface temperature at sub-satellite FOV.

Determination of the reflectance/temperature of pure ice pixels is the key to calculate the ice concentration. In a square search window with a size of 50 by 50 pixel, reflectance/temperature probability density function (PDF) is calculated using all the ice covered pixels detected in the first step described in section 3.4.2.1. The size of the search window is an algorithm parameter. This PDF is presented as histogram bins as a function of surface reflectance/temperature. For temperature, the minimum bin value is 215 K, with bin width 0.5 K, total bin number 121. For reflectance, the minimum bin value is 0., with bin width 0.02, total bin number 121 to be consistent with the total bin number of temperature. The histogram bins are then smoothed by a running boxcar filter with a width of 5 bins, in which a sliding integral is calculated over the original PDF. A new smoothed PDF is derived as the result. The ice reflectance/temperature tie

point is chosen as the reflectance/temperature with the maximum probability density in the smoothed PDF, i.e. the maximum sliding integral. The reason that the location of the max PDF point is selected as the tie point of pure ice is that ice with 100% ice concentration is assumed to be majority in a search window, and the ice characteristics are homogeneous in the search window. The tie point algorithm described above is adapted from an algorithm by Appel and Kenneth (2002). The tie point reflectance of open water is parameterized as a function of solar zenith angle, with 0.05 for solar zenith angle less than 65 degree and 0.07 for solar zenith angle larger than or equal to 65 degree. The tie point surface temperature of open water changes with the water salinity, 273.15 K for freshwater and 271.5 K for salt water.

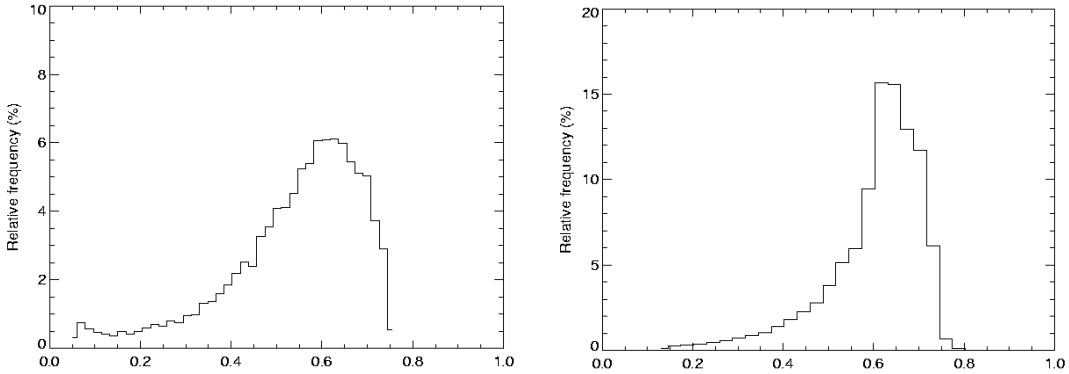

Figure 2. *Left: Reflectance probability density distribution at 0.64 μm for ice cover over Lake Erie on Feb 24, 2008. Right: Reflectance probability density distribution at 0.64 μm for ice cover over Barents and Kara Seas, March 31, 2008.*

3.4.2.3 Ice cover

Ice cover is determined by ice detection tests. As the first step, pixels with ice detected using daytime tests are assigned value 1, and value 2 at nighttime when only surface skin temperature test is used. Pixels with water covered are assigned value -2. Land and cloud pixels are assigned value -1 and 0 respectively. The default value of ice cover is -3.

Users can refine the ice mask with retrieved ice concentration. For example, after ice concentration is retrieved, pixels assigned value 1 or 2 after the first step can be re-assigned value -2 (water surface) if the retrieved ice concentration less than 15%.

3.5 Algorithm Output

Outputs of this algorithm are:

- Ice Concentration
- Ice Cover
- Ice Surface Temperature
- Quality control (QC) flags
- Metadata

These are described in Tables 11 and 12.

Table 11. *Output and additional output parameters and their definitions.*

Definition	**Description**	**Unit**
Ice concentration	The fraction (in percentage) of the sea or lake surface covered by ice	Unitless
Ice cover	A pixel is ice covered or not. Value 1: ice detected using daytime tests 2: ice detected using nighttime tests 0: cloud -1: land -2: water surface -3: non-retrievable due to sunglint, cloud shadow, and missing pixels	Unitless
Ice surface temperature (additional)	Skin temperature at ice surface	Kelvin

Table 12. *Ice Cover and Concentration Quality Information (4 bytes)*

Byte	Bit	Quality Flag Name	Description	Meaning
1	0	QC_output	Output product quality	00 - good 01 - uncertain 10 – non-retrievable 11 – bad data
	1			
	2	QC_INPUT_CLD	Input cloud mask	00 - clear 01 - probably clear 10 -probably cloudy 11-cloudy
	3			
	4	QC_INPUT_DAY	Day/Night	0-Day 1-Night
	5	QC_INPUT_SUNGLINT	Sunglint or not	0-Yes 1-No
	6	QC_INPUT_CLDSHADOW	Cloud shadow or not	0-Yes 1-No
	7	empty		
2	0	QC_INPUT_SOLZEN	Valid solar zenith angle (0-180 degree)	0-Yes 1-No

	1	QC_INPUT_SATZEN	Valid satellite zenith angle (0-180 degree)	0-Yes 1-No
	2	QC_INPUT_REFL	Valid reflectance at 0.47 μm (0.0-1.0)	0-Yes 1-No
	3		Valid reflectance at 0.64 μm (0.0-1.0)	0-Yes 1-No
	4		Valid reflectance at 0.86 μm (0.0-1.0)	0-Yes 1-No
	5		Valid reflectance at 1.6 μm (0.0-1.0)	0-Yes 1-No
	6	QC_INPUT_THERMAL	Valid brightness temperature at 10 μm (100-390 k)	0-Yes 1-No
	7		Valid brightness temperature at 11 μm (100-390 k)	0-Yes 1-No
3	0	QC_INPUT_SURFACE	Surface type flag	00 - in-land water 01 - sea water 10- land 11 – others
	1			
	2	QC_TEST_REFL	Success of reflectance test in ice cover detection	0-Yes 1-No
	3	QC_TEST_NDSI	Success of NDSI test in ice cover detection	0-Yes 1-No
	4	QC_TEST_SKINTEMP	Success of skin temperature test in ice cover detection	0-Yes 1-No
	5	QC_TIE_REFL	Success of visible band tie-point algorithm	0-Yes 1-No
	6	QC_TIE_SKINTEMP	Success of skin temperature tie-point algorithm	0-Yes 1-No
	7	empty		
4	0	QC_READ_INPUT	Success in reading input	0-Yes 1-No
	1			
	2			
	3			
	4			

	5			
	6			
	7			

Metadata can be derived from quality information of the output. The metadata include the common metadata for all data products and specific metadata for ice cover and concentration product.

Common metadata for all data products:

- DateTime (swath beginning and swath end)
- Bounding Box
  - Product resolution (nominal and/or at nadir)
  - Number of rows, and number of columns
  - Bytes per pixel
  - Data type
  - Byte order information
  - Location of box relative to nadir (pixel space)
- Product Name
- Product units
- Ancillary data to produce product (including product precedence and interval between datasets is applicable)
  - Version Number
  - Origin
  - Name
- Satellite
- Instrument
- Altitude
- Nadir pixel in the fixed grid
- Attitude
- Latitude, longitude
- Grid projection
- Type of scan
- Product version number
- Data compression type

- Location of production
- Citations to documents
- Contact information

Ice Cover and Concentration Specific Metadata can include:

- Number of QA flag values (currently, there are 4: Normal or Optimal; Uncertain or Suboptimal; Non-retrievable; Bad data)
- For each QA flag value, the following information is provided:
  - Definition of QA flag
  - Total pixel numbers with the QA flag
- Total number of pixels with water surface
- Total number of valid ice cover and concentration retrievals (good and uncertain)
- Total percentage of valid ice cover and concentration retrievals of all pixels with water surface
- Total pixels numbers and percentage of terminator pixels (Non-retrievable and Bad data)
- Pixel number of daytime ice cover and concentration valid retrievals
- Pixel number of nighttime ice cover and concentration valid retrievals
- Mean, Min, Max, and standard deviation of valid ice concentration retrievals
- Pixel size of search window to determine tie-point.

4 Validation

4.1 Validation of products using proxy data

Proxy data of GOES-R ABI and VIIRS used to test this algorithm included observations from MODIS and Spinning Enhanced Visible & InfraRed Imager (SEVIRI) onboard of the MSG (Meteosat Second Generation) satellites. The channels in the proxy data associated with GOES-R ABI are listed in Table 13. Validations were performed by comparison to passive microwave ice cover and concentration product from Advanced Microwave Scanning Radiometer - Earth Observing System (AMSR-E), comparison with true-color satellite images, and comparison with ice cover and ice concentration of ice chart from National Ice Center and Environment Canada, which are detailed in the following subsections. Our testing and validations include both sea and lake ice.

Table 13. *Channels in the proxy data of GOES-R ABI.*

ABI Band Number	***ABI Wavelength (μm)***	***MODIS band v (Wavelength μm)***	***SEVIRI band (Wavelength μm)***
2	0.64	1 (0.64)	1 (0.635)
3	0.86	2 (0.86)	2 (0.81)
5	1.61	6 (1.6)	3 (1.64)
14	11.2	31 (11)	9 (10.80)
15	12.3	32 (12)	10 (12.0)

4.1.1 MODIS Data

MODIS is a key instrument onboard the Terra (*EOS AM, refer to http://terra.nasa.gov/*) and Aqua (*EOS PM, refer to http://aqua.nasa.gov/*) satellites. Terra's orbit around the Earth is timed so that it passes from north to south across the equator in the morning, while Aqua passes south to north over the equator in the afternoon. The MODIS instrument has a viewing swath width of 2,330 km and views the entire surface of the Earth every one to two days. Its detectors measure 36 spectral bands between 0.405 and 14.385 μm, and it acquires data at three spatial resolutions - 250m, 500m, and 1,000m.

Figure 3 shows an example of sea ice concentration retrievals from MODIS data as the proxy of GOES-R ABI and VIIRS. Figure 3(a) shows the ice concentration retrieval based on tie point algorithm from MODIS retrieved ice surface temperature, and Figure 3(b) shows the ice concentration retrieval based on tie point algorithm from MODIS visible band reflectance at 0.64 μm. Both retrievals show similar results, with high sea ice concentration near the North Pole and lower values towards the ice edges. Figure 4 shows an example of ice concentration retrieval over the Great Lakes and inland waters from MODIS observations. The retrieved ice concentration agrees well with the patterns observed from the MODIS true color image.

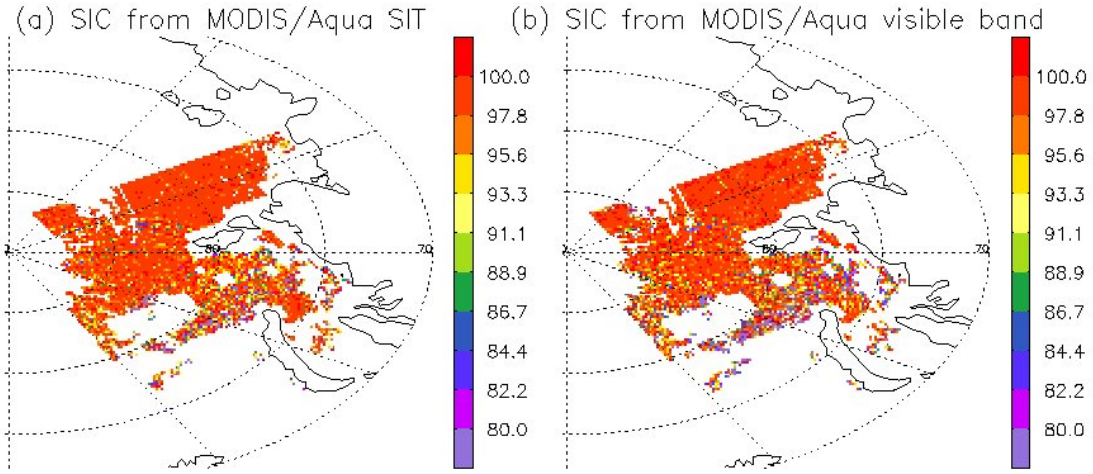

Figure 3. *Sea ice concentration (SIC) (%) retrieved from (a) MODIS Sea Ice Temperature (SIT), (b) MODIS visible band (0.64 μm) reflectance using tie point algorithm on March 31, 2006.*

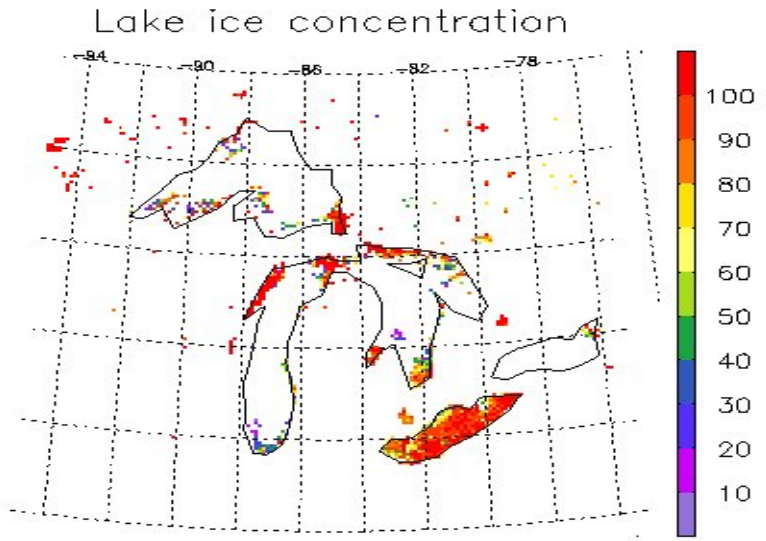

Figure 4. *Lake ice concentration (%) with MODIS Aqua visible band (0.64 μm) data on February 24, 2008.*

4.1.2 SEVIRI Data

SEVIRI is the primary payload of the MSG satellites, which form a joint project between the European Space Agency and Eumetsat, the European Organisation for the Exploitation of

Meteorological Satellites since 1977 (*refer to http://www.eumetsat.int/home/Main/Access_to_Data/Meteosat_Image_Services/SP_1123237865326*). SEVIRI measures reflected and emitted radiance in 11 spectral channels located between 0.6 μm and 14 μm with a nominal spatial resolution of 3 km at the sub-satellite point along with an additional broadband high-resolution visible (0.4-1.1 μm) channel that has a 1 km spatial resolution. The full disk view allows frequent sampling, every 15 minutes, enabling monitoring of rapidly evolving events. The nominal coverage includes the whole of Europe, Africa and locations at which the elevation to the satellite is greater than or equal to 10°.

Figure 5 shows an example of ice concentration retrievals over the Caspian Sea from SEVIRI observations. Figure 5(a) shows the retrieval based on SEVIRI retrieved ice surface temperature, and Figure 5(b) shows the ice concentration retrieval based on SEVIRI visible band reflectance at 0.64 μm. Both retrievals show similar results, with higher ice concentration over the northern part, decreasing southward, and eventually open water. Comparison of the retrieved ice concentration to those observed from satellite true color image show good agreement, which demonstrates that this ice concentration retrieval algorithm works for lake ice concentration retrieval using SEVIRI data.

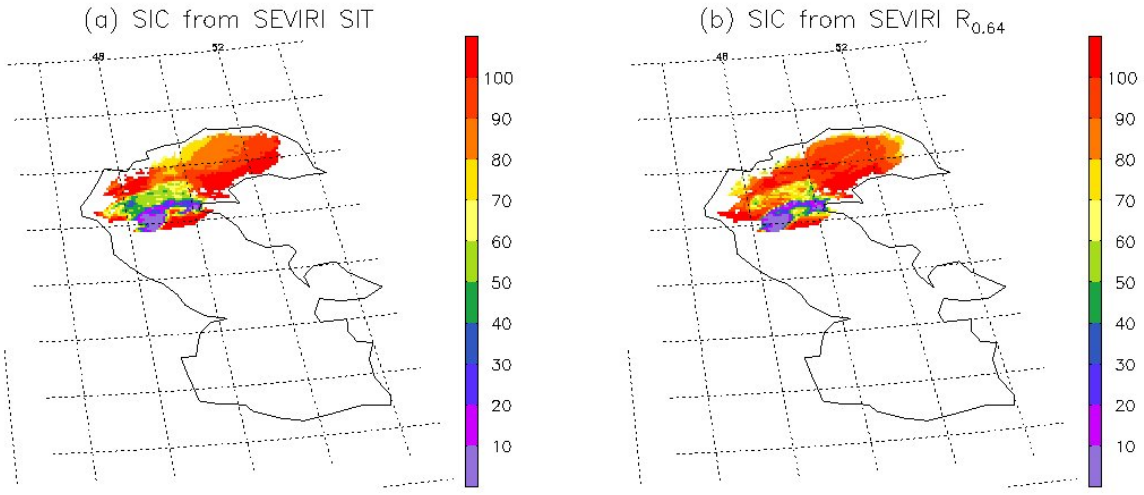

Figure 5. *Lake ice concentration (%) retrieved from (a) SEVIRI Surface Ice Temperature (SIT), (b) SEVIRI visible band reflectance (0.64 μm) on January 27, 2006.*

4.1.3 Precisions and Accuracy Estimates

Product measurement accuracy requirement for ice cover is 85% correction detection. The product measurement accuracy requirement for ice concentration is 10%, with a product measurement precision requirement of 25%. Direct match ups and comparison between satellite retrieved ice cover and concentration and satellite true color images are done to gain qualitative results. Comparison of the retrieved products with ice cover and concentration from passive

microwave products, and ice chart provides quantitative results, with mean bias, standard deviation, and bias frequency distribution.

4.1.3.1 Comparison with AMSR-E

The AMSR-E instrument onboard Aqua Satellite is a twelve-channel, six-frequency, conically-scanning, passive-microwave radiometer system. It measures horizontally and vertically polarized microwave radiation (brightness temperatures) ranging from 6.9 GHz to 89.0 GHz. Spatial resolution of the individual measurements varies from 5.4 km at 89 GHz to 56 km at 6.9 GHz. The AMSR-E instrument provides measurements of land, oceanic, and atmospheric parameters, including sea ice concentration, snow water equivalent, and etc.

The AMSR-E Level-3 gridded product (AE_SI12) includes sea ice concentration mapped to a polar stereographic grid at 12.5 km spatial resolution. This dataset is used for comparison with the sea ice concentration retrievals using MODIS as proxy data.

Figure 6 shows an example of comparison of sea ice concentration from AMSR-E product and from MODIS. Both products show similar patterns in the sea ice concentration, high values in the central Arctic and lower value towards to Barents Sea. The MODIS retrievals show more details in the central Arctic in correspondence to leads in the sea ice. The MODIS retrievals also show lower sea ice concentration towards the open water. Although AMSR-E is not ground truth, statistical estimates of difference between these sea ice concentrations provide helpful information of the retrieval algorithm. The MODIS sea ice concentrations were averaged for 11x11 pixels (native resolution is 1 km at the sub-satellite point) centered on the AMSR-E footprint (about 12 km nadir). For this specific case, the bias and standard deviation between AMSR-E and MODIS surface skin temperature (reflectance) based sea ice concentration are 2.8% (5.6%), and 4.1% (7.5%).

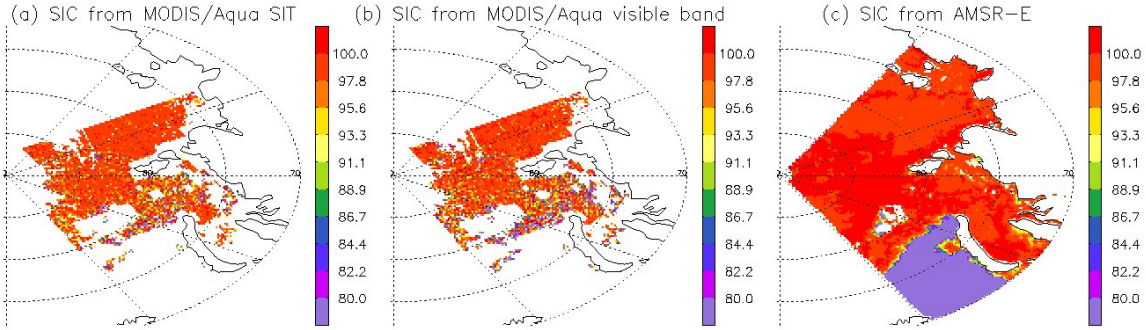

Figure 6. *Sea ice concentration (SIC) (%) retrieved from (a) MODIS Sea Ice Temperature (SIT), (b) MODIS visible band reflectance, and (c) from Advanced Microwave Scanning Radiometer - Earth Observing System (AMSR-E) Level-3 gridded daily mean from NSIDC on March 31, 2006.*

4.1.3.2 Comparison with the satellite true color images

Lake ice concentrations are also compared with the satellite true color images for qualitative purpose. Though these comparisons cannot give quantitative results, it helps to show whether the retrieved ice cover and concentration have reasonable distributions.

Figure 7 gives an example of comparison of MODIS retrieved lake ice concentration with satellite true color image. The lake ice cover determined from satellite observations shows good agreement with that inferred from the satellite true color image, as well as the general distribution of ice concentration. Ice concentration retrieved using MODIS data show better ice concentration distributions, e.g. over Lake Erie, than those from AMSR-E.

Figure 7. *Lake ice concentration (%) with MODIS Aqua data (left, MODIS true color image (middle), and ice concentration from AMSR-E (right) over Great Lakes on February 24, 2008.*

4.1.3.3 Comparison with ice chart

The Interactive Multisensor Snow and Ice Mapping System (IMS) began to generate daily snow and ice cover products at spatial resolution of 4 km in the Northern Hemisphere since 2004 in National Ice Center (http://nsidc.org/data/docs/noaa/g02156_ims_snow_ice_analysis/). This product has been used to validate the ice cover retrievals both over the Great Lakes and over the Arctic Ocean using this algorithm on MODIS data.The bi-weekly ice charts generated in National Ice Center also provides Arctic ice concentration at spatial resolution of 25 km (http://nsidc.org/data/docs/noaa/g02172_nic_charts_climo_grid/index.html). This dataset has also been used to validate the ice concentration retrievals over the Arctic Ocean using this algorithm on MODIS data.

4.1.3.4 Error Budget

Retrieved ice cover and concentration using MODIS data as proxy over the Arctic of 41 days evenly distributed in four seasons, and over the Great Lakes of similar number of days are compared with ice concentration product from AMSR-E, and ice chart as truth.

A pixel is determined as not ice covered if the AMSR-E sea ice concentration is lower than 15%. Comparisons show that the correct detection ratio of ice cover is 87.6% (Table 14), which is higher than the required measurement accuracy for ice cover. The bias and standard deviation of retrieved ice concentration are –4.0% (4.0%) and 25.6% (15.7%) over the Great Lakes (Arctic

Ocean) compared with AMSR-E ice concentration (Table 15). Histogram of these two ice concentration differences is shown in Figure 8. Results show ice concentration retrievals using MODIS data as proxy meet the ice cover correct detection ration, 85%, and concentration accuracy and precision requirement, 10% and 25%, in regard to comparison with AMSR-E product as truth.

***Table 14**: Performance of ice cover product compared with AMSR-E*

Case Number Total pairs: 1576298	Sea/Lake ice cover determined from AMSR-E	Water surface determined form AMSR-E
Sea/Lake ice cover determined using this algorithm	1075124	
Water surface determined using this algorithm		305872
Correct detection ratio = (1075124+305872)/1576298 = 87.6%		

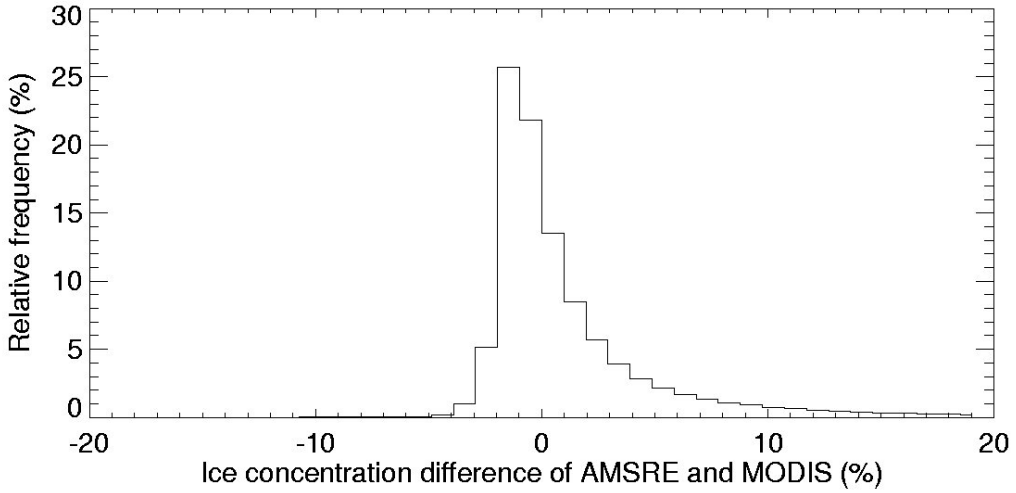

***Figure 8.** Frequency distribution of ice concentration difference between AMSRE product and retrievals using this algorithm based on selected 41 day MODIS data in four seasons in 2007 over the Arctic Ocean.*

***Table 15.** Performance of retrieved ice concentration compared with AMSR-E.*

Ice concentration difference of AMSR-E product and MODIS product as proxy of GOES-R ABI	Mean bias (%)	Standard Deviation (%)
Over Arctic Ocean	4.0	15.7
Over Great Lakes	-4.0	25.6

Required Measurement Accuracy	10	
Required Measurement Precision		25

Matches are found between retrieved ice concentration using this algorithm on MODIS data and ice chart over ten million for ice cover both over the Great Lakes and the Arctic Ocean. Over one hundred thousand for ice concentration over the Arctic Ocean. Results show that the correct detection ratio of ice cover is 91.5%, which is higher than the required measurement accuracy for ice cover. The bias and standard deviation of retrieved ice concentration are –1.2% and 15.7% over the Great Lakes, and 9.5% and 15.7% over the Arctic Ocean, which meets the ice concentration accuracy and precision requirement, 10% and 25%.

4.2 Validation of products using VIIRS

This algorithm has been running using S-NPP VIIRS data. Figure 9 shows the VIIRS IST on December 9, 2015 for one overpass over the Arctic and for a daily Arctic composite using all the overpasses in that day. Figure 10 shows the ice concentration on December 9, 2015 for one overpass and daily composite.

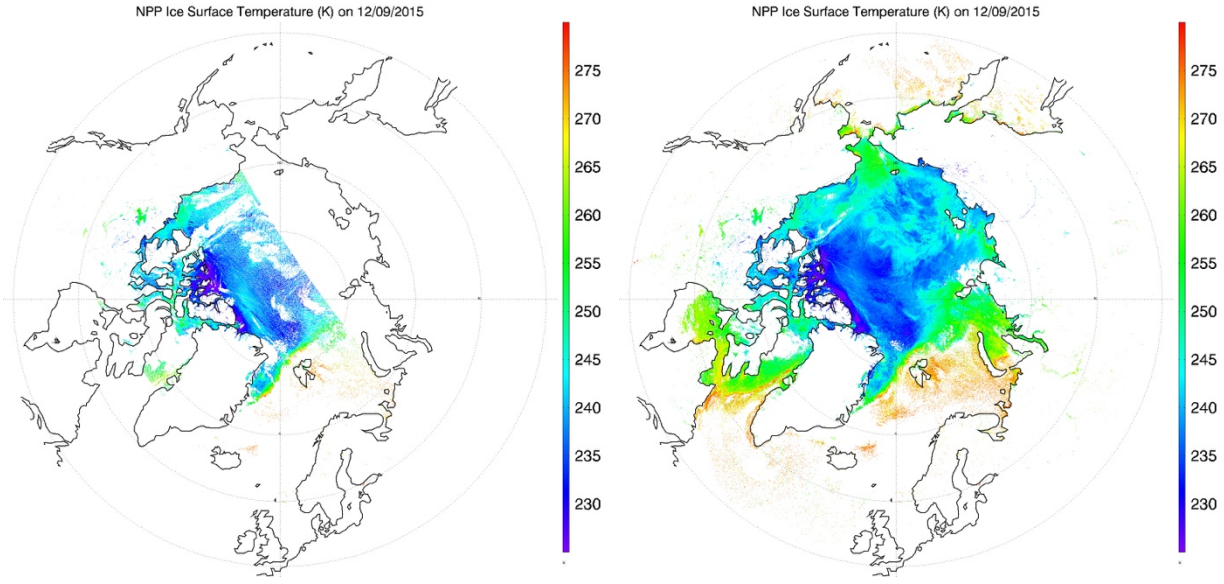

Figure 9. L*eft: Ice surface temperature (IST) for VIIRS overpass over the Arctic from 10:57 to 11:15 UTC on December 9, 2015. Right: Daily IST composite over the Arctic on December 9, 2015.*

Quality of the S-NPP VIIRS IST has been being routinely examined and monitored. Validation is performed through comparisons with multiple datasets, including NASA IceBridge measurements, air temperature from Arctic drifting ice buoys, and MODIS IST. IST data sets from MODIS, specifically the Terra MODIS (MOD29) and Aqua MODIS (MYD29) Sea Ice

Extent 5-Min L2 Swath 1 km datasets (Hall and Riggs 2015) are used to compare with the S-NPP VIIRS IST. These MODIS data sets are in swath format at 1 km resolution at nadir for both daytime and nighttime under clear sky conditions. To collocate the VIIRS IST and MODIS IST, every overpass over the Arctic and Antarctic of the VIIRS IST and MODIS IST are re-gridded to a 1 km Equal-Area Earth Grid (EASE-Grid) using map projection tool MODIS Swath-to-Grid Toolbox (MS2GT), with 9025 by 9025 grid cells extending from 48.4 to 90°N over the Arctic and 8025 by 8025 grid cells extending from 53.2 to 90°S over the Antarctic. Only cases with VIIRS and MODIS observation time differences of less than 5 minutes are selected for monitoring. Figure 11 shows the IST from MODIS Aqua and VIIRS on December 5, 2015. Both retrievals show similar pattern and values.

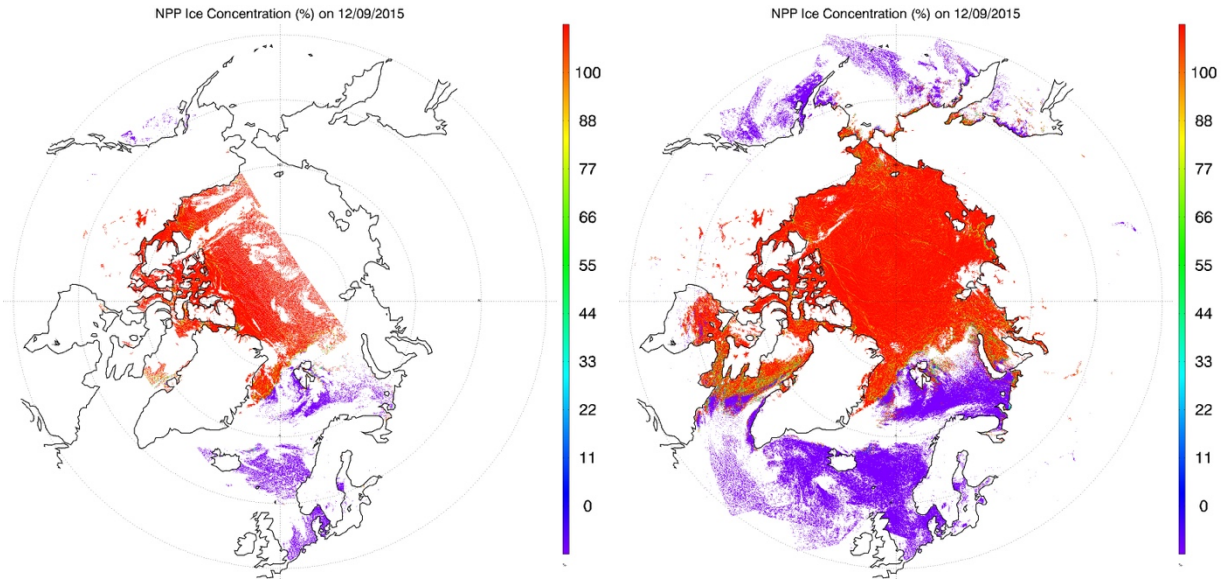

Figure 10. *Left: Ice concentration for VIIRS overpass over the Arctic from 10:57 to 11:15 UTC on December 9, 2015. Right: Daily ice concentration composite over the Arctic on December 9, 2015.*

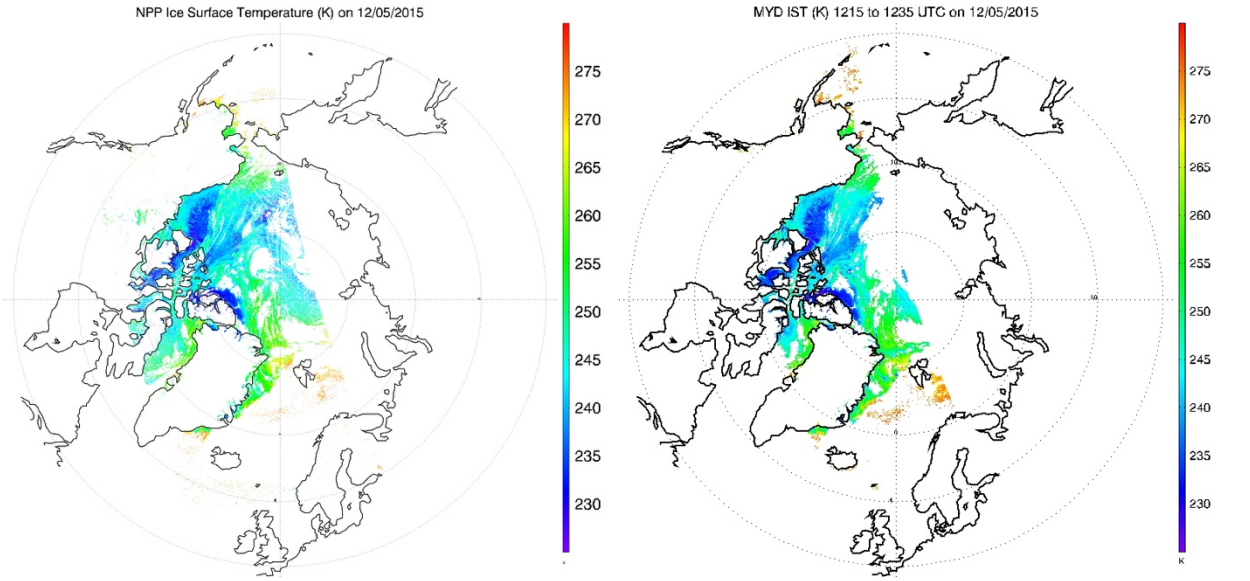

Figure 11. *Ice concentration for VIIRS (left) from 12:13 to 12:31 UTC, and Aqua MODIS (right) from 12:15 to 12:35 UTC on December 5, 2015.*

IST has been measured with an airborne Heitronics KT-19.85 Series II infrared radiation pyrometer (KT-19) on a National Aeronautics and Space Administration (NASA) P3 craft during the NASA Operation IceBridge campaigns (Krabill and Buzay 2014). The validation of the VIIRS IST with KT-19 IST measurements provides the most accurate assessment of VIIRS IST quality. All KT-19 observations in the Arctic from 2013 to 2015, and 2017, are used to validate collocated VIIRS IST. All available KT-19 temperature measurements that are within 375 m of the center of the VIIRS pixel are averaged. Only KT-19 temperature samples with standard deviations less than 2 K are used in matchup comparisons in order to eliminate cases with small-scale IST outliers that VIIRS would not be able to resolve. In addition, the closest KT-19 point to the VIIRS pixel must be within 15 minutes and 100 meters to be considered. Finally, a rigorous quality control is done to make sure that the VIIRS IST value is not contaminated by cloud. With the collocated VIIRS IST EDR and KT-19 IST over the Arctic, the VIIRS accuracy is 0.282 K, with a precision of 0.993 K (Figure 12). It should be noted that the IceBridge KT-19 measurements are concentrated in the springtime. More measurements from other seasons, when the IST is near the melting point or is very low, are desirable.

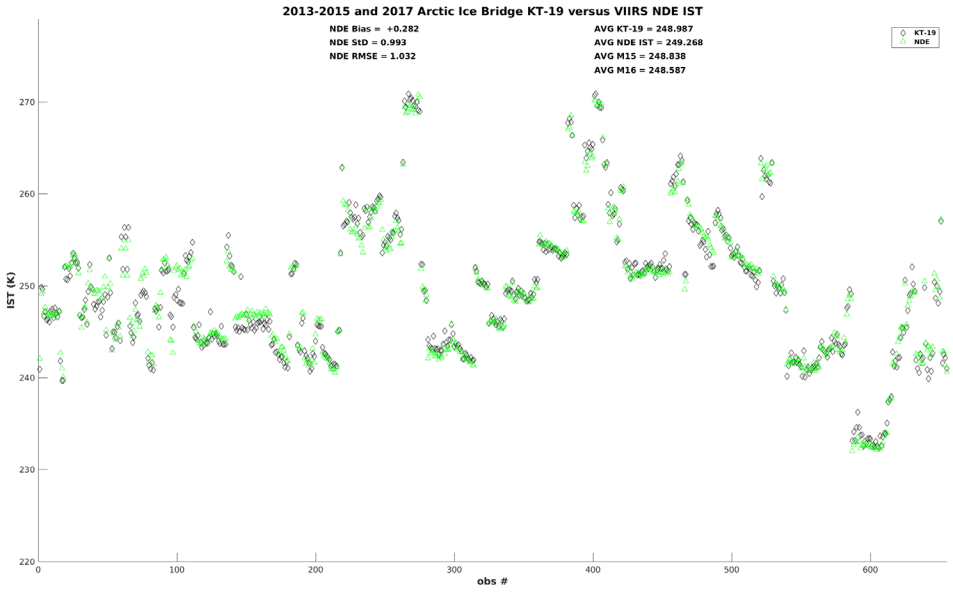

Figure 12. *VIIRS IST (green) and KT-19 IST (black) for all coincident IceBridge flights with cloud-free observations over the Arctic from 2013 to 2015, and 2017.*

Quality of the sea ice concentration and ice cover are being monitored routinely and examined with other datasets. Quality of VIIRS sea ice concentration is being monitored using collocated sea ice concentration retrievals from the Special Sensor Microwave Imager/Sounder (SSMIS) onboard the Defense Meteorological Satellite (DMSP) F17 satellite processed with the NASA Team Algorithm (Cavalieri et al. 1999). This product contains daily sea ice concentrations at a resolution of 25 km for both hemispheres. Sea ice concentration retrievals from VIIRS and the daily passive microwave product are collocated through remapping to a 25 km EASE-Grid with the nearest neighbor interpolation for the passive microwave data, and a weighted average for VIIRS. An example of the collocated VIIRS and passive microwave sea ice concentration on December 9, 2015 is shown in Figure 13. Both products show similar overall spatial distributions, with VIIRS ice concentration shows more spatial details. A reduction in the sea ice concentration from the pack ice to the ice edge shown in the microwave product is not shown in the VIIRS product, which can partly be attributed to the differences in instrument sensitivities, instrument field-of-view, and the fundamental differences in the retrieval algorithms.

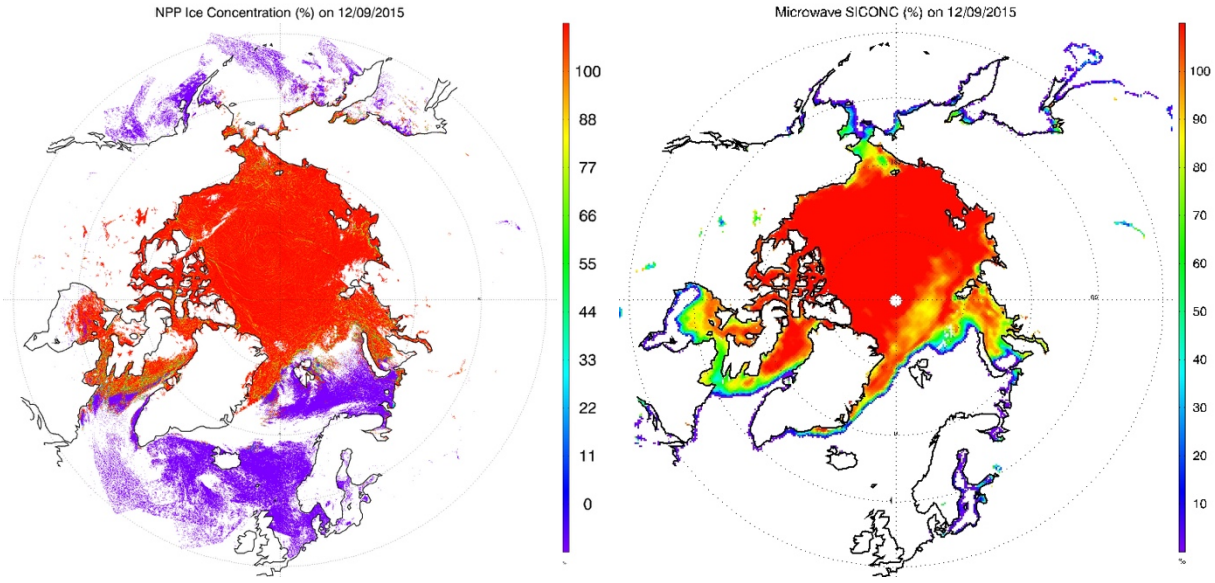

Figure 13. *Ice concentration for daily ice concentration composite from VIIRS (left) and from microwave using NASA team algorithm (right) over the Arctic on December 9, 2015.*

Validation of VIIRS sea ice concentration has been done by using high-resolution Landsat data. All Landsat 8 scenes in the year 2013 and 2014 that contain Arctic sea ice and are 90% or more clear sky covered are ordered from the U.S. Geological Survey (USGS) data sever. There are totally 181 Landsat scenes. In each scene, each pixel has visible and thermal channel observation at 30 m spatial resolution from the Operational Land Imager (OLI) and the Thermal Infrared Sensor (TIRS). Each pixel at the original spatial resolution is determined as either snow/ice or water under clear conditions based on the visible channel reflectance and the derived NDSI. Sea ice concentration at lower spatial resolutions of 1 km, 6.25 km, and 25 km is calculated as the ratio of snow/ice pixel number to all pixel number inside a grid cell of 1 km, 6.25 km, and 25 km. For each of the Landsat scene, a correspondent S-NPP VIIRS ice concentration with time difference less than 1 hour is collocated. Figure 14 shows a collocated Landsat ice concentration and S-NPP VIIRS ice concentration at 1 km spatial resolution. A daily mean sea ice concentration product is also sought from the Advanced Microwave Scanning Radiometer 2 (AMSR2) at 6.25 km using NASA 2 algorithm, and from SSMIS at 25 km using NASA algorithm. These four SICs are remapped to 6.25 km EASE-Grid (not for SSMIS). Accuracy and precision of S-NPP VIIRS ice concentration are calculated in regard to ice concentration from Landsat (Figure 15). The overall accuracy and precision of the S-NPP VIIRS ice concentration are 1.11% and 10.61%.

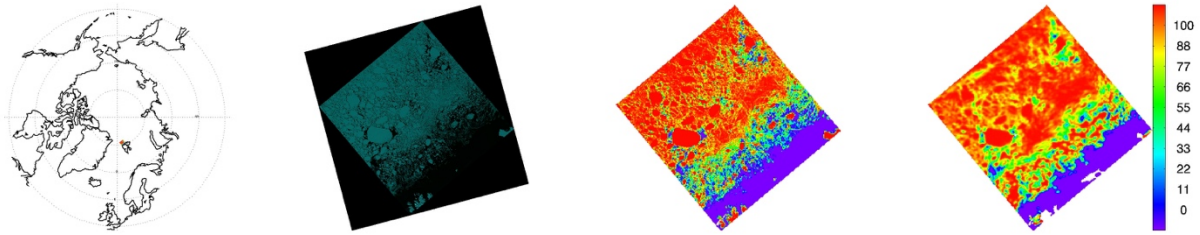

Figure 14. *From left to right: location of the scene shown; true color image of Landsat; Landsat sea ice concentration; and S-NPP VIIRS ice concentration at 12:09 UTC on May 27, 2013.*

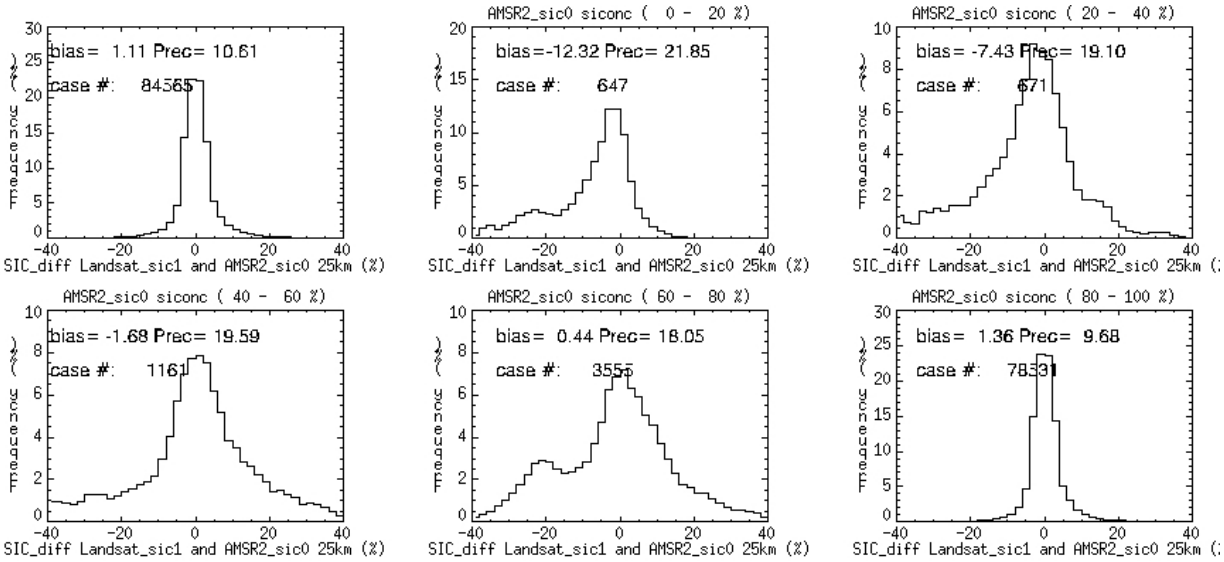

Figure 15. *Comparison of VIIRS and Landsat ice concentrations for different concentration ranges/bins with bias and RMSE with bias removed (precision).*

These validation and evaluation results demonstrate the high quality of the VIIRS IST and ice concentration as indicated by the absolute accuracy and precision values in regard to comparison with the IceBridge KT-19 measurement, and Landsat ice concentration. Based on the IceBridge and Landsat results, the VIIRS IST and ice concentration accuracy and precision meets or exceeds the JPSS system requirement.

4.3 Validation of products using GOES-R ABI

4.3.1 Mitigation of the GOES-17 Loop Heat Pipe subsystem issue

"During post-launch testing of the GOES-17 ABI instrument, an issue with the instrument's cooling system was discovered. The loop heat pipe (LHP) subsystem, which transfers heat from the ABI electronics to the radiator, is not operating at its designed capacity. The consequence of

this is that the ABI detectors cannot be maintained at their intended temperatures under certain orbital conditions. Inadequate cooling of the infrared channels leads to partial loss of imagery during some of the overnight hours before and after the vernal and autumnal equinoxes.

Infrared signals with long wavelengths can be swamped by infrared light emitted by warm parts of the imager, degrading the signal. Cooling the detectors reduces this thermal "noise" in observations. During some nighttime hours during certain parts of the year (before and after the vernal and autumnal equinoxes), the sun heats up seven of the ABI detectors faster than they can be cooled. The detectors become warmer than they're designed to operate, and they begin to radiate at temperatures closer to the wavelengths they're attempting to detect from the Earth. Eventually, local emissions and dark current noise overwhelm the signal from the Earth, and the channels saturate, meaning a useful signal is not available." (https://www.goes-r.gov/users/GOES-17-ABI-Performance.html).

To mitigation this LHP issue in the ice products, the following approach is taken. Metadata of "DQF", 'percent_good_pixel_qf', in L1b data is read in as input. All the radiance data is set as missing if 'percent_good_pixel_qf' less than a set threshold, 0.99. The rational is that the 'percent_good_pixel_qf', the ratio of good pixels to all pixels, is usually higher than 0.99 when the LHP is working normally. When the LHP temperature regulation anomaly starts, that ratio starts to decrease. When the ratio is less than 0.99, all the input data is set as missing, so that ice products will not be generated for the whole image.

4.3.2 Validation for ABI

This algorithm has been running using ABI data. Figure 16 shows an example of derived ABI ice concentration on February 14, 2018 in Full Disk view, and Figure 17 is the derived ABI ice concentration on the same day over the Great Lakes region, with white color representing area without retrievals due to cloud cover and other factors. The retrieval shows generally higher ice concentration near the lake shore and in the bay area, e.g. the shore of the Lake Michigan and the Green Bay, and over the Lake Erie, and lower ice concentration far away from shore. Qualitative evaluation of GOES-R ABI ice concentration has been carried out with comparison to ABI true-color images. As an example, Figure 18 shows the natural-color image of ABI on February 14, 2018. The derived ABI ice concentration agrees with the pattern of ice concentration distribution inferred from the image. Quantitative evaluation of ABI ice concentration from February 1 to 28, and from April 17 to 30, 2018 is performed with comparison to ice concentration from passive microwave observations, i.e. the AMSR2 (Advanced Microwave Scanning Radiometer 2) ice concentration at 10.0 km spatial resolution using NASA team 2 algorithm. Both ice products are remapped to 4 km EASE-Grid using nearest-neighbor approach. Analysis of collocated ice products shows that the correct detection ratio of ice cover is 99.95% (Table 16), which is higher than the required measurement accuracy for ice cover. The accuracy and precision of the ABI ice concentration are 1.87% and 7.81% (Table 17). Results show ice concentration retrievals using ABI meet the ice cover correct detection ration, 85%, and concentration accuracy and precision requirement, 10% and 25%, in comparison with AMSR2 product.

Figure 16. *Derived ABI ice concentrations on February 14, 2018 in full disk.*

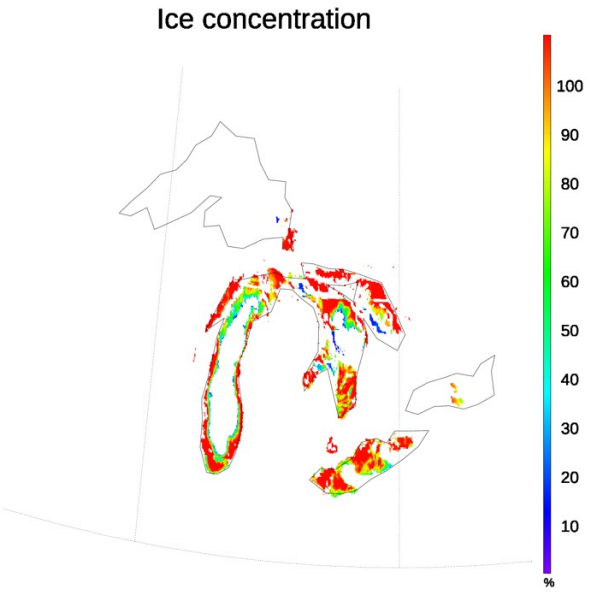

Figure 17. *Derived ABI ice concentrations on February 14, 2018 over the Great Lakes.*

Figure 18. *ABI natural-color composite image on February 14, 2018 over the Great Lakes.*

Table 16*: Performance of ABI ice cover product compared with AMSR2*

Case Number Total pairs: 20741717	Sea/Lake ice cover determined from AMSR2	Water surface determined form AMSR2
Sea/Lake ice cover determined using this algorithm	20731626	7843
Water surface determined using this algorithm	2218	30
Correct detection ratio = (20731626+30)/20741717 = 99.95%		

Table 17. *Performance of retrieved ABI ice concentration compared with AMSR2.*

Ice concentration difference of AMSR2 product and ABI product	Mean bias (%)	Standard Deviation (%)
	1.87%	7.81%
Required Measurement Accuracy	10	
Required Measurement Precision		25

4.4 Products using METimage

Three overpasses of METimage proxy data are provided by EUMETSAT, covering from 8:43 to 10:23 UTC, from 10:23 to 12:05 UTC on September 12, 2007, and from 8:46 to 10:29 UTC on February 23, 2008 respectively. Radiance data are provided, with geolocation and ancillary data, including longitude, latitude, solar and satellite viewing angles, land-water mask, and cloud mask. Radiance data are converted to visible reflectance and brightness temperatures. Figure 18 shows reflectance at 0.64 μm and brightness temperature at 10.69 μm (BT11) of overpass from 10:23 to 12:05 UTC on September 12, 2007.

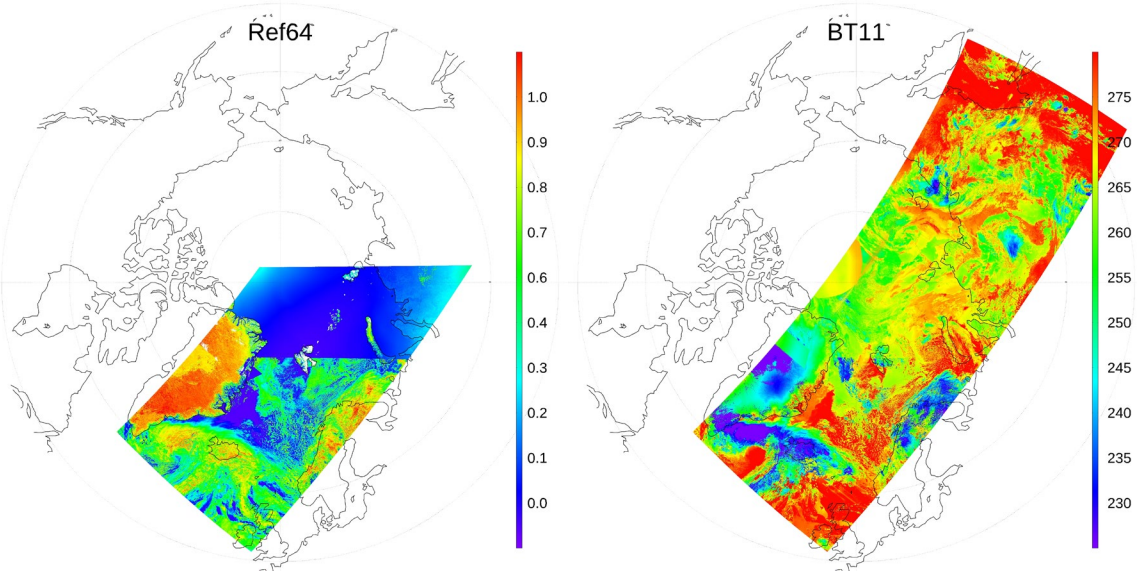

Figure 19*.Reflectance at 0.64 □m (left) and brightness temperature at 10.69 □m (BT11)(right) of overpass from 10:23 to 12:05 UTC on September 12, 2007.*

This algorithm runs on the EPS-SG proxy data. In the calculation of ice surface temperature, the retrieval coefficients for S-NPP VIIRS are used for that the spectral response functions of METimage (or VII) are not yet available. All other parameters are the same as those for VIIRS. Figure 20 shows the derived ice concentration and ice surface temperature for the overpass from 10:23 to 12:05 UTC on September 12, 2007. Validation of the products from the three overpasses and possible more overpasses in the future will be carried out.

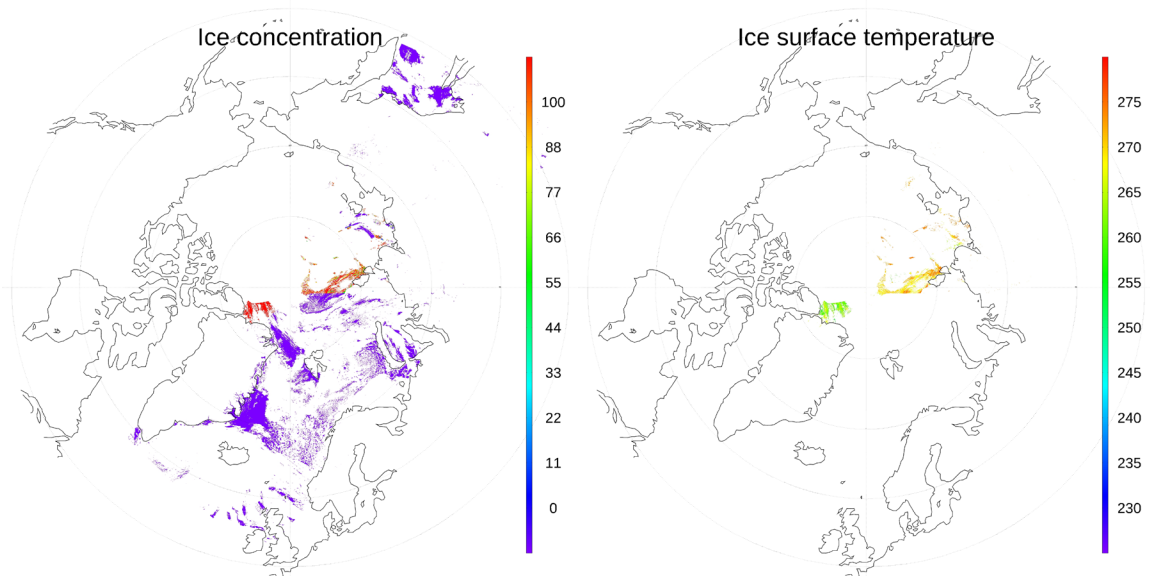

Figure 20. *Derived ice concentration (left) and ice surface temperature (right) of overpass from 10:23 to 12:05 UTC on September 12, 2007.*

5 Practical Considerations

5.1 Numerical Computation Considerations

This ice cover and concentration algorithm is implemented sequentially. The computation time is very economic.

5.2 Programming and Procedural Considerations

This ice cover and concentration algorithm requires spatial information in a search window. Temporal information from previous observations is not necessary.

5.3 Quality Assessment and Diagnostics

Describe how the quality of the output products and the retrieval itself is assessed, documented, and any anomalies diagnosed.

The following procedures are recommended for diagnosing the performance of this algorithm.

- Check input data such as BTs, and reflectance for all pixels.
- Check the inputs from cloud mask, and land mask.
- Monitor the products automatically with other products from different satellite, and real time in-situ observations.
- Periodically check images of individual test results to look for artifacts or non-physical behaviors.

- Maintain a close collaboration with other teams, which use the output of this algorithm in their product generation and other applications.

5.4 Exception Handling

This algorithm includes checking the validity of input data before running and setting quality flag for the input data and in the output product. This algorithm also checks for missing input variables values. In this case, correspondent flag is set to indicate that no ice cover and concentration were produced for that pixel.

5.5 Algorithm Validation

This algorithm is validated using products from MODIS and SEVIRI data as proxy data, and products from S-NPP VIIRS and GOES-R ABI. Accuracy and precision of ice concentration and ice surface temperature, and correct detection rate of ice cover are calculated. Validations with other data sets show that products meet the MRD required accuracy and precision. More extensive validation will be carried out over ocean and the inland waters, in comparison with in situ measurements, and ice products from AMSR2, ice chart, and satellite instruments with very high spatial resolution.

6 Assumptions and Limitations

The following sections describe limitations and assumptions in the current version of this algorithm.

6.1 Assumptions

The following assumptions have been made in developing and estimating the performance of this algorithm. The following list contains the current assumptions and proposed mitigation strategies.

1. Cloud mask eliminates all possible cloud contamination.
2. Land mask maps are available to identify different surface types.
3. Changes of reflectance/temperature in a search window are mainly due to difference in ice concentration on pixel level. Viewing angles in a search window do not change much considering the size of the search window. Pixels with 100% ice cover are majority in a search window.

We assume the sensor will meet its current specifications, and retrieved products from other teams will be accurate enough for this algorithm.

As for sensitivity estimates, a source error 0.5 K (0.01) in surface skin temperature (visible channel reflectance) leads to around 2% (2%) error in ice concentration, for tie point ice surface skin temperature (visible reflectance) being 250 K (0.55).

6.2 Limitations

Limitations of this algorithm includes

1. Ice concentration is not retrieved if less than 10% of all pixels in a search window is covered by ice, in which tie-point reflectance or surface temperature of pure ice cannot be determined. However, ice cover can still be identified. Quality flags are set in the final ice concentration product for this condition.
2. The assumption that 100% ice cover pixels are majority in a search window can be violated under some conditions. When partially ice-covered pixels are more than 100% ice-covered pixels, the final ice concentration may have higher uncertainties.

6.3 Planned Product Improvements

Further tuning of this algorithm, including ice detection test thresholds, new possible detection tests, and improvement in the tie-point algorithm may be needed. Routine quantitative validation with in situ measurements, and passive microwave ice products, ice products from sensors with higher spatial resolution, and ice chart will continue to be carried out over both sea and inland water.

Development of this algorithm is closely tied to the algorithm development and feedback from other teams. Future improvement will be dependent on the feedback and suggestions from other teams and users of this product.

7 References

Appel I., and J. A. Kenneth, 2002, Fresh water ice Visible/Infrared Imager/Radiometer Suite algorithm theoretical basis document, Version 5. SBRS document #: Y2404.

Bolsenga, S.J. 1983, Spectral reflectances of snow and fresh-water ice from 340 through 1100 nm. *J. Glaciology*, 29(102), 296-305.

Cavalieri, D. J., C. l. Parkinson, P. Gloersen, J. C. Comiso, and H. J. Zwally. 1999. Deriving Long-term Time Series of Sea Ice Cover from Satellite Passive-Microwave Multisensor Data Sets. *Journal of Geophysical Research* 104(7): 15,803-15,814.

Grenfell, T. C. and G. A. Maykut, 1977, The optical properties of ice and snow in the Arctic Basin, *J. Glaciol.*, 18, 445-63.

Hall, D. K. and G. Riggs. 2015. *MODIS/Terra Sea Ice Extent 5-Min L2 Swath 1km, Version 6*. Boulder, Colorado USA. NASA National Snow and Ice Data Center Distributed Active Archive Center. http://dx.doi.org/10.5067/MODIS/MOD29.006.

Hall, D. K. and G. A. Riggs. 2015. *MODIS/Aqua Sea Ice Extent 5-Min L2 Swath 1km, Version 6*. Boulder, Colorado USA. NASA National Snow and Ice Data Center Distributed Active Archive Center. http://dx.doi.org/10.5067/MODIS/MYD29.006.

Hall D.K., G.A. Riggs, and V.V. Salomonson, 2001, Algorithm theoretical basis document for the MODIS snow and sea ice mapping algorithms.

Hall D.K., G.A. Riggs, and V.V. Salomonson, 2006, MODIS sea ice products user guide to collection 5.

Key, J., J. Collins, C. Fowler, and R. Stone, 1997, High-latitude surface temperature estimates from thermal satellite data. Remote Sensing Environ., 61, 302-309.

Krabill, W.B.; Buzay, E. updated 2014. IceBridge KT-19 IR Surface Temperature, Version 1. [2012-2015]. **2012**, Boulder, Colorado USA. NASA National Snow and Ice Data Center Distributed Active Archive Center. http://dx.doi.org/10.5067/I883KXU7ZO8O

Lindsay, R. W., and D. A. Rothrock 1995, Arctic sea ice leads from advanced very high resolution radiometer images, J. Geophys. Res., 100, 4533-4544.

Riggs G.A., D.K. Hall, and S.A. Ackerman, 1999, Sea ice extent and classification mapping with the Moderate Resolution Imaging Spectroradiometer Airborne Simulator. Remote Sensing of Environ., 68, 152-163.

Schmit, Timothy J., Mathew M. Gunshor, W. Paul Menzel, James J. Gurka, Jun Li, A. Scott Bachmeier, 2005: Introducing the next-generation Advanced Baseline Imager on GOES-R. Bull. Amer. Meteor. Soc., 86, 1079-1096